Response to Reviewers

Dear editor and reviewers:

Thank you very much for your letter and the constructive comments concerning our manuscript, now entitled "*Impacts of synoptic circulation types on nocturnal ozone increase in the North China Plain: Meteorological drivers and physical mechanisms*" (Manuscript ID: egusphere-2026-25).

We deeply appreciate the time and effort you have dedicated to reviewing our work. The insightful feedback has been exceedingly valuable in refining our terminology, strengthening our scientific arguments, and improving the overall quality of the paper. We have carefully considered all the comments and revised the manuscript accordingly.

General Update: Please note that to ensure absolute terminological rigor and to perfectly align with the reviewers' excellent suggestions, we have slightly adjusted the title from "...formation mechanisms" to "...physical mechanisms".

Please find below our detailed point-by-point responses to the specific comments as follows:

Reviewers' comments are in black.

Authors' responses are in blue.

Changes in the manuscript are in red.

Your Sincerely,

Liya Fan,

On behalf of the authors

Reviewer #1

Major comments:

1. The authors selected only four stations in Xinxiang City for their study and further identified 197 days during which NOI events occurred simultaneously at all stations as a representative sample. Why do these four stations, which are located relatively close to one another, have more days with non-overlapping NOI events than days with overlapping events? If the NOI is primarily driven by large-scale atmospheric circulation, why did the four sites not experience simultaneous events? This strongly suggests the dominant role of local emissions or mesoscale processes, making the authors' subsequent focus on the analysis of large-scale atmospheric circulation appear to lack a solid foundation.

Response 1: Thanks for reviewer's comments. The ultimate occurrence of NOI is indeed inextricably linked to localized boundary-layer and mesoscale processes. Rather than contradicting our focus on synoptic circulations, this physical reality is the exact theoretical foundation for our specific sampling strategy.

Our detailed rationale is as follows, which we have now clarified in the revised manuscript:

(1) We deliberately selected these four stations for two critical reasons. First, high representativeness: they are all official state-controlled environmental monitoring stations (national network). Collectively, they provide a highly representative spatial footprint of the city's core urban environment. Second, robust data completeness: compared with other regional sub-stations, these four state-controlled stations exhibit the highest data integrity and continuity over our long-term study period, ensuring the robust quality of our observational basis and preventing any single-site measurement bias.

(2) Physical meaning of non-overlapping events (filtering random noise): Local emissions and highly isolated micro-topographic eddies can trigger NOI at individual sites. However, these non-overlapping events represent highly localized, decoupled random noise (e.g., a random emission plume or a strictly localized sub-grid eddy). Analyzing these days would obscure the systematic physical mechanisms we aim to reveal.

(3) Core paradigm (macro-to-micro scale): We strictly selected days with simultaneous NOI events across all four stations not to neglect local boundary-layer physics, but to ensure that the local boundary-layer changes were systematically driven by a unified macro-scale forcing. When

NOI occurs simultaneously across the entire urban footprint, it strongly implies a macro-to-micro scale cascade: a powerful synoptic-scale forcing (e.g., massive subsidence, strong advection) successfully and universally triggered the necessary localized boundary-layer turbulence (e.g., enhanced mechanical wind shear, U^* spikes) across the entire region.

(4) Solidifying the foundation: Our representative sample isolates the events where large-scale atmospheric circulations act as the overarching commanders, while localized boundary layer dynamics act as the executors. Focusing our Lamb-Jenkinson weather classification and mechanistic analysis on this specific subset provides a rigorous foundation for revealing how different synoptic patterns uniquely modulate local boundary layer mechanics to trigger NOI.

This rationale was not sufficiently articulated in the original manuscript, which led to the misunderstanding. We have now explicitly added this justification in the Section 2.3 to clarify the scientific premise of our sampling strategy.

Lines 92-93:

In this study, these four stations were deliberately selected due to their strong spatial representativeness over the urban core and their high data completeness.

Lines 234-242:

It is worth noting that non-overlapping NOI events frequently occur among the different stations, highlighting the inevitable influence of random localized emission noise and uncoordinated micro-environmental fluctuations. To rigorously isolate the overarching synoptic-scale meteorological drivers from these random local chemical/emission noises, this study specifically focused on representative events where NOI occurred simultaneously across all stations. Rather than neglecting local boundary-layer processes, these simultaneous occurrences serve as robust indicators of powerful regional episodes. They demonstrate that the large-scale synoptic forcing was sufficiently intense to synchronize the local boundary-layer dynamics (e.g., vertical wind shear and turbulent mixing) across the entire urban region. This rigorous screening ensures that the localized physical mechanisms evaluated in subsequent sections are systematically driven by macro-weather types, rather than coincidental local perturbations.

2. The authors did not specify whether they used meteorological fields covering the entire day for

Lamb-Jenkinson classification. The fundamental flaw in this approach is that the classification is based on average atmospheric circulation throughout the day or at specific times, whereas NOI is a short-term phenomenon occurring during specific hours at night.

Response 2: Thanks for reviewer's comments. Daytime data is heavily dominated by intense solar radiation and daytime convective boundary layer dynamics, blurs and misrepresents the actual synoptic forcing present during the exact nocturnal hours when the O_3 enhancement is triggered.

To resolve this issue and strictly align the synoptic background with the NOI occurrences, we have discarded the daily average approach and recalculated the Lamb-Jenkinson (L-J) classification using strictly nocturnal meteorological fields.

Furthermore, to ensure the utmost methodological rigor and to completely exclude any potential boundary layer convective perturbations near sunrise, we implemented a seasonally-adjusted nocturnal window based on local sunrise times:

(1) For April to September, where sunrise occurs earlier (after 05:00 LT), we averaged the meteorological fields from 20:00 LT to 05:00 LT the following day.

(2) For October to March, where sunrise occurs later (after 06:00 LT), the nocturnal window was extended from 20:00 LT to 06:00 LT the following day.

Using these nighttime sea level pressure (SLP) fields, we re-ran the L-J classification for all representative NOI days. Consequently, all subsequent analyses, including the frequencies of weather types, meteorological characteristic, and mechanistic discussions, have been comprehensively updated.

Lines 143-146:

To accurately capture the synoptic background driving NOI events and to eliminate daytime boundary layer convective perturbations, the classification was performed using strictly nocturnal SLP fields rather than daily averages. Furthermore, a seasonally-adjusted nocturnal window was applied based on local sunrise times, consistent with the nocturnal time window adopted for NOI.

3. Lines 87–92: If I understand correctly, the author defines an NOI event as a rise in hourly O_3 concentration during the night exceeding 10 μg m^{-3} compared to the previous hour. This definition does not account for the diurnal cycle of O_3 concentrations. Between 00:00 and 06:00, as sunrise approaches and temperatures rise, O_3 concentrations naturally tend to increase. If the diurnal cycle

is not accounted for, a significant portion of the detected so-called NOI events may simply be part of normal daily variations.

Response 3: Thanks for reviewer's comments. We have re-evaluated our identification framework to ensure the diurnal cycle is strictly accounted for, addressing reviewer's concerns through two targeted steps:

(1) Clarifying on the concentration changes of normal nocturnal O_3:

Extensive literatures (He et al., 2022; Zhu et al., 2020; Wang et al., 2025; Nair et al., 2002) establish that in the absence of solar radiation, nocturnal O_3 concentrations normally exhibit a continuous decrease from 20:00 LT until sunrise. This is driven by NO titration and surface dry deposition. The normal, sunlight-driven diurnal rebound of surface O_3 typically does not begin until 06:00–08:00 LT (depending on the season). Therefore, a sudden, short-term spike exceeding 10 μg m^{-3} occurring in the deep night (e.g., between 00:00 and 04:00 LT) is highly anomalous. It is distinctly not a part of the normal daily variation but is primarily driven by physical transport mechanisms (such as downward mixing from the residual layer).

(2) Eliminating of the approaching sunrise interference:

As summer approaches, sunrise occurs earlier (e.g., before 06:00 LT). If the identification window extends to 06:00 LT during these warmer months, there is a genuine risk that the detected O_3 increase might be partially contaminated by early-morning photochemical production rather than purely nighttime dynamic transport. To rigorously eliminate this false-positive threat and completely isolate our analysis from the daytime diurnal cycle, we redefined our NOI identification window using the same seasonally-adjusted strategy mentioned in our response to Comment 2:

For April to September, since sunrise is earlier, we strictly truncated the identification window to 20:00-05:00 LT the following day.

For October to March, the window remained at 20:00-06:00 LT the following day.

Lines 126-129:

Considering the seasonal variation in local sunrise time, we excluded NOI events occurring after 05:00 LT from April to September, when the sunrise occurs relatively early. Since nighttime generally lasts from 20:00 to 06:00 LT the next day, it constitutes a continuous process. Therefore, a day is classified as an NOI day if such events occur from 20:00 to 06:00 LT the next day (excluding April to September, for which the window is 20:00 to 05:00 LT).

4. The grouping of weather types is overly subjective and lacks quantitative justification, resulting in ambiguity regarding the physical significance of the categories. The authors subjectively grouped the 23 weather types generated by the Lamb-Jenkinson method into four major categories: A-type, C-type, S-type, and WNE-type. The rationale for this grouping is stated as being "based on the position of central system and different meteorological elements of each classification", but this has not been quantified or clearly explained in the manuscript.

Response 4: Thanks for reviewer's comments. The original manuscript lacked a rigorous, quantitative explanation for grouping the Lamb-Jenkinson weather types into four major categories (A, C, S, and WNE). The primary objective of this grouping was to reduce dimensionality and extract the overarching physical mechanisms driving NOI, but we realize that the lack of explicit quantitative justification made the process appear subjective.

To rectify this and provide a robust quantitative foundation, we have made our grouping criteria completely transparent, based rigorously on the objective physical properties of the synoptic systems (specifically, SLP anomalies and geostrophic wind vorticity):

(1) Quantitative grouping criteria:

A-type (Anticyclonic group): This category quantitatively lumps all subtypes characterized by strong anticyclonic vorticity and positive SLP anomalies dominating the North China Plain (e.g., Pure A, and hybrid A types like AE, AW). Physically, these are unified by their shared capacity to induce broad regional subsidence.

C-type (Cyclonic group): This lumps subtypes dominated by cyclonic vorticity and negative SLP anomalies (e.g., Pure C, and hybrid C types), unifying them through their shared dynamic triggering of localized convective downdrafts or atmospheric instability.

S-type (Southerly group) & WNE-type (West-North-East group): The directional types were categorized quantitatively based on the dominant azimuth of the geostrophic wind vectors and the strong orientation of the pressure gradient force, representing distinct horizontal advection and shear-induced mixing profiles.

(2) Quantitative verification (new composite analysis & analysis of variance):

To definitively eliminate any ambiguity regarding their distinct physical significance, we conducted two major additions to the revised manuscript:

Composite synoptic patterns (new Fig. 5): We calculated the composite mean fields (SLP and 850 hPa wind vectors) for these four major categories. These composites were calculated strictly using the seasonally-adjusted nocturnal window. The newly added Fig. 5 unequivocally demonstrates that the four groups possess fundamentally distinct synoptic pressure distributions and low-level advection characteristics.

Statistical significance test (Fig. 6 and Table S2): We conducted a One-Way Analysis of Variance (ANOVA) on the nocturnal anomalies of key local meteorological variables (T, RH, WS, PBLH and U^*) across the four groups. As shown in the new Fig. 6 and Table S2, the inter-group differences are highly statistically significant (all $p < 0.01$). This firmly proves that our classification objectively separates fundamentally different boundary layer thermodynamic environments.

Lines 276-282:

Notably, to extract the overarching dynamical mechanisms and reduce the statistical noise of the 20 specific Lamb-Jenkinson weather types, we quantitatively clustered them into four major archetypes: Anticyclonic (A-type), Cyclonic (C-type), Southerly (S-type), and West-North-East (WNE-type). Rather than subjective grouping, this clustering was rigorously based on their shared physical topology: specifically, the polarity of SLP anomalies, geostrophic vorticity, and the primary azimuth of geostrophic wind vectors. The detailed quantitative criteria for each of the four weather types are provided in Text S2. To further validate the physical distinctness of this categorization, composite analysis of the synoptic fields and Analysis of Variance (ANOVA) on localized boundary layer variables were conducted.

Lines 283-296:

To verify that the four grouped weather types possess fundamentally distinct atmospheric backgrounds, we analyzed their composite mean SLP and 850 hPa wind fields (Fig. 5). The spatial distributions unequivocally demonstrate distinct synoptic forcings: A-type is dominated by a strong, uniform high-pressure center over the study region (Fig. 5(a)); C-type is characterized by cyclonic curvature and low-pressure system (Fig. 5(b)); S-type is driven by intense southerly advection between a western low and an eastern high (Fig. 5(c)); and WNE-type features strong northeasterly flows driven by a massive continental high to the northwest (Fig. 5(d)). Furthermore, to statistically

confirm that these different synoptic structures translate into distinctly different local thermodynamic environments, a One-Way ANOVA was performed on the nocturnal anomalies of key meteorological variables (T, RH, WS, PBLH and U^*) across the four groups. The resulting statistical distributions and data spreads are visually compared in Fig. 6, while the precise quantitative parameters and significance test results are detailed in Table S2. To strictly isolate the meteorological perturbations driven by synoptic systems and to eliminate the influence of seasonal and interannual backgrounds, the nocturnal anomalies (Δ) for key meteorological variables were calculated as the difference between the NOI days' specific nocturnal average and the corresponding monthly nocturnal mean. The results show that the inter-group differences are highly statistically significant (all $p < 0.01$), definitively proving that our quantitative classification objectively separates fundamentally different boundary layer environments.

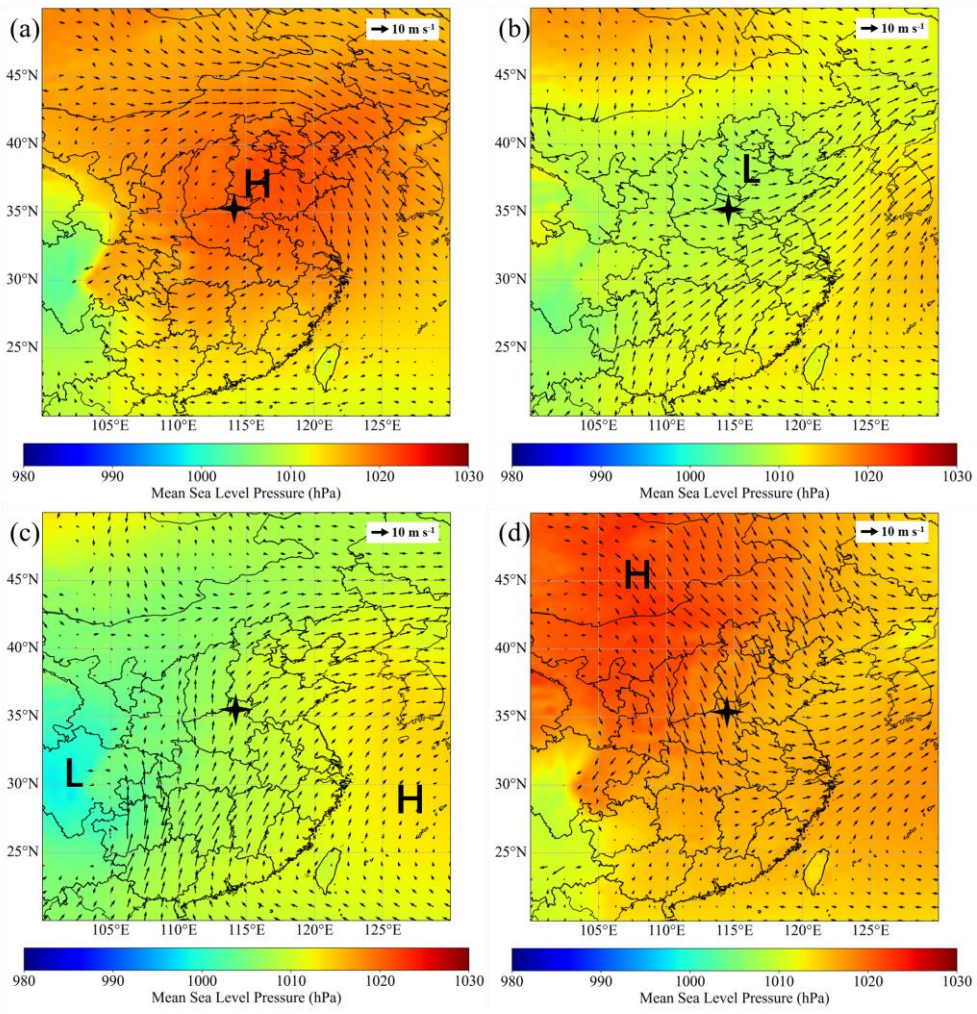

Figure 5: Spatial distribution of composite mean SLP and 850 hPa wind fields under different weather categories: (a) A-type, (b) C-type, (c) S-type, (d) WNE-type (asterisk indicates the location of Xinxiang; "H" and "L" stand

for high-pressure and low-pressure, respectively).

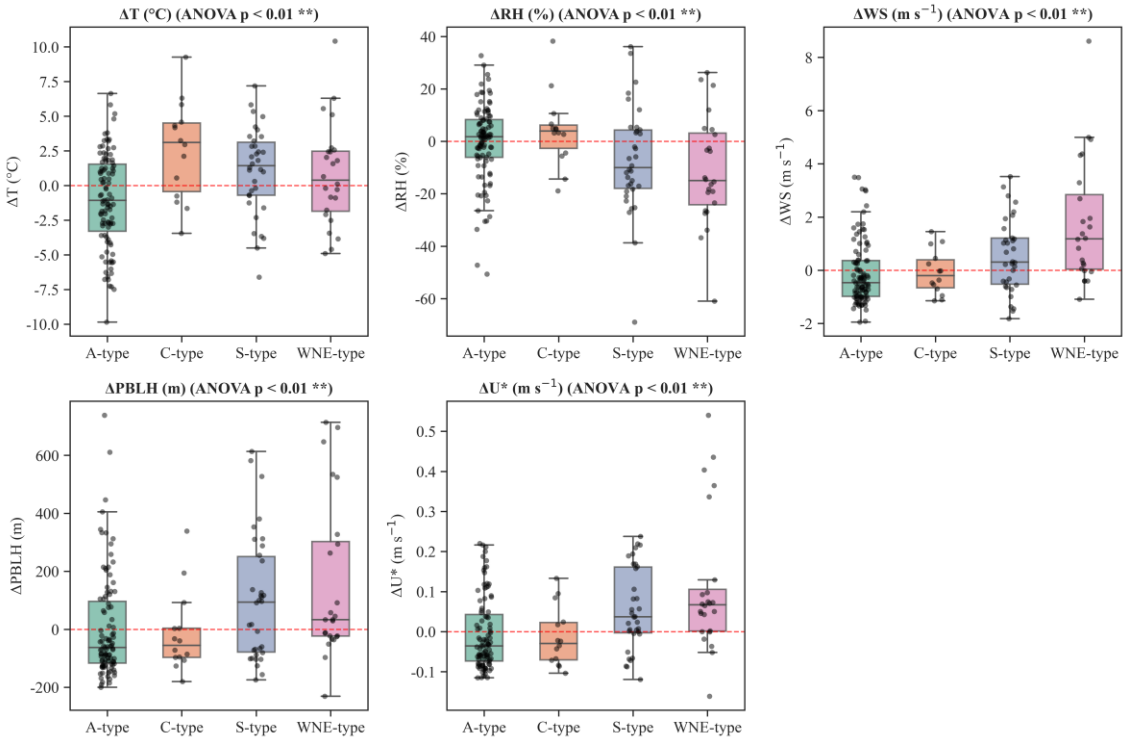

Figure 6: One-Way ANOVA results for key meteorological variables (T, RH, WS, PBLH and U^*) of different synoptic categories. In each boxplot, the central black solid line indicates the median. The horizontal red dashed line denotes the zero-anomaly reference.

Table S2. Statistical summary of nocturnal meteorological anomalies and ANOVA results under the four weather types.

Variable	A-type	C-type	S-type	WNE-type	p-value
ΔT (°C)	-1.07 ± 3.41	2.60 ± 3.54	1.06 ± 3.18	0.77 ± 3.70	$< 0.01^{**}$
ΔRH (%)	-0.31 ± 14.82	4.08 ± 14.00	-7.12 ± 20.46	-11.15 ± 20.72	$< 0.01^{**}$
ΔWS (m s^{-1})	-0.10 ± 1.21	-0.08 ± 0.83	0.54 ± 1.39	1.74 ± 2.32	$< 0.01^{**}$
ΔPBLH (m)	3.56 ± 178.15	-14.44 ± 139.19	102.41 ± 216.82	156.22 ± 274.82	$< 0.01^{**}$
ΔU^* (m s^{-1})	-0.01 ± 0.09	-0.01 ± 0.07	0.06 ± 0.10	0.11 ± 0.17	$< 0.01^{**}$

Note: Data are presented as Mean ± Standard Deviation. The anomalies (Δ) were calculated relative to their respective monthly nocturnal means. The p-values are derived from One-Way ANOVA tests indicating statistical significance under the four weather types.

Text S2: Quantitative grouping criteria.

(1) A-type (Anticyclonic group): This category quantitatively lumps all subtypes characterized

by strong anticyclonic vorticity and positive SLP anomalies dominating the North China Plain (e.g., Pure A, and hybrid A types like AE, AW). Physically, these are unified by their shared capacity to induce broad regional subsidence.

(2) C-type (Cyclonic group): This lumps subtypes dominated by cyclonic vorticity and negative SLP anomalies (e.g., Pure C, and hybrid C types), unifying them through their shared dynamic triggering of localized convective downdrafts or atmospheric instability.

(3) S-type (Southerly group) & WNE-type (West-North-East group): The directional types were categorized quantitatively based on the dominant azimuth of the geostrophic wind vectors and the strong orientation of the pressure gradient force, representing distinct horizontal advection and shear-induced mixing profiles.

5. The logic of the entire Section 3.3 is inverted. Rather than analyzing how the specific meteorological conditions of each weather type led to NOI, the author devotes a significant amount of space to explaining how the meteorological conditions of each type contribute to the maintenance of atmospheric circulation. Of greater interest is which local meteorological variables (such as temperature, wind, and boundary layer height) directly drive the formation of NOI within the context of already classified atmospheric circulation.

Response 5: Thanks for reviewer's comments. The original Section 3.3 mistakenly focused on the climatological maintenance of the synoptic systems across different seasons, rather than explicitly elucidating the local meteorological drivers of NOI.

To correct this fundamental flaw, we have completely rewritten Section 3.3. We removed the extensive discussions on seasonal climate maintenance. We redirected the entire focus toward analyzing: how the specific local meteorological variables (temperature, wind, relative humidity, and boundary layer height) directly drive the thermodynamic and kinematic environment for NOI under the classified circulations.

To provide robust, quantitative evidence, we integrated the composite synoptic maps (Figs. 5 and 7) with the rigorously calculated nocturnal anomalies of local variables (Fig. 6 and Table S2). The revised Section 3.3 is presented below:

Lines 307-367:

3.3 Meteorological characteristics of primary weather types

As established in Section 3.1, the vast majority of NOI events in Xinxiang occur during the LN period. During this phase, the nocturnal boundary layer is characterized by a fully established surface inversion, creating a highly stable thermodynamic environment. To trigger downward O_3 transport under such extreme stability, localized residual turbulence is entirely insufficient. Instead, it requires massive, active mechanical forcing capable of physically breaking the inversion layer. Because such powerful mechanical triggers are fundamentally governed by macro-scale weather systems, identifying the specific synoptic circulations is the critical next step to unravel the forcing mechanisms behind these NOI events.

It should be noted that while seasonal variations significantly influence the daytime photochemical generation and absolute background concentrations of O_3, the nocturnal occurrence of NOI is predominantly driven by physical transport. As validated by the seasonal comparison (Fig. S6 and Text S3), while the absolute intensity of meteorological variables naturally fluctuates across seasons, the fundamental dynamical frameworks for a given weather type (e.g., the general orientation of horizontal pressure gradients and patterns of vertical motions) maintain functionally comparable mechanical triggers. Therefore, rather than focusing on seasonal background variations, our study focuses on elucidating these primary, synoptically-driven local meteorological drivers that trigger NOI.

The representative NOI days in Xinxiang were classified into four weather types (A-type, C-type, S-type, and WNE-type), with each exhibiting distinct meteorological features. Fig. 7 illustrates the spatial distributions of 850 hPa wind fields under four weather types. Under A-type, Xinxiang was located near a high-pressure center, with an outward-rotating wind field at 850 hPa (Figs. 5(a) and 7(a)), indicating the presence of an anticyclonic high-pressure system. Driven by this synoptic forcing, Xinxiang experienced extremely calm conditions. As explicitly demonstrated by the nocturnal anomalies in Fig. 6 and Table S2, A-type was characterized by negative anomalies in wind speed (mean: $\Delta WS = -0.10$ m s^{-1}) and friction velocity (mean: $\Delta U^* = -0.01$ m s^{-1}), alongside a strongly constrained boundary layer (mean: $\Delta PBLH = 3.56$ m, representing negligible expansion). This indicates that the overriding high-pressure system creates a highly stable environment. The explicit intrusion process of O_3 under this subsidence will be further verified in Section 3.4.

Under C-type, Xinxiang was dominated by low-pressure systems (Fig. 5(b)). At 850 hPa, a strong airflow originating near the coastal region of Guangxi Province moved continuously

northeastward (Fig. 7(b)). This airflow not only moved at a high speed, but also likely carried substantial moisture, significantly enhancing atmospheric instability in its trajectory and surrounding regions (including Xinxiang), intensifying convective activity, and increasing the risk of heavy rainfall. Combined with the water vapor flux and divergence fields at 850 hPa, we find that the intense southwest warm-wet moisture transport belt under C-type is extremely prominent. Significant moisture convergence is observed along the entire path of this belt (including Xinxiang) (Fig. S7). Notably, the local meteorological anomalies perfectly capture this advection, with C-type uniquely coinciding with distinct positive anomalies in temperature (mean: $\Delta T = 2.60$ °C) and the highest relative humidity anomaly among all weather types (mean: $\Delta RH = 4.08\%$). This localized warm and highly humid environment, dynamically coupled with a cyclonic low-pressure background, significantly amplifies atmospheric thermodynamic instability, highly favoring the development of regional convection and precipitation. Consequently, rather than uniform large-scale subsidence, NOI under C-type is primarily triggered by convective downdrafts and the subsequent development of cold pools.

S-type represents a dynamic environment driven by distinct horizontal advection. Under S-type, Xinxiang was situated in a tight pressure gradient, typically between a western low and an eastern high (Figs. 5(c) and 7(c)). Driven by this synoptic setup, continuous southerly geostrophic winds prevailed over the region. As detailed in Table S2, S-type produced significant positive anomalies in local wind speed (mean: $\Delta WS = 0.54$ m s^{-1}) and friction velocity (mean: $\Delta U^* = 0.06$ m s^{-1}). These specific values rigorously demonstrate that beyond facilitating regional horizontal transport (which will be explicitly traced in Section 3.4.1), the southerly advection directly generates substantial localized mechanical turbulence at the surface, physically lifting the nocturnal boundary layer (mean: $\Delta PBLH = 102.41$ m). This localized mechanical shear serves as the direct trigger for breaking nocturnal stability, subsequently entraining O_3-rich air from the elevated residual layer down to the surface and triggering NOI events.

Although Xinxiang often featured a massive continental high-pressure system (e.g., the Siberian High) to the northwest under WNE-type (Fig. 5(d)), their local dynamics are fundamentally different from the pure subsidence of A-type. At 850 hPa, the region was obviously influenced by a northwestern airflow (Fig. 7(d)), consistent with the geostrophic wind characteristics of WNE-type. Unlike A-type, where the study area sits calmly at the high-pressure

center, under WNE-type, Xinxiang was located at the densely packed periphery of the advancing high. Consequently, the macroscopic forcing shifts to intense horizontal pressure gradients (Figs. 5(d) and 7(d)). This kinematic distinction is perfectly captured by the localized surface anomalies (Table S2). WNE-type exhibited the most extreme positive anomalies among all categories, with local wind speed (mean: ΔWS = 1.74 m s^{-1}) and friction velocity (mean: ΔU^* = 0.11 m s^{-1}) far exceeding other types. Driven by this intense horizontal advection and wind shear, the nocturnal boundary layer experienced massive mechanical lifting (mean: $\Delta PBLH$ = 156.22 m). Furthermore, this intense mechanical mixing effectively breaks the nocturnal surface inversion, bringing slightly warmer air from aloft downward (detailed mechanism analysis is presented in Section 3.4.2). This vigorous downward mixing of the elevated residual layer shares conceptual similarities with the nocturnal fumigation-like processes documented in other literature (Wu et al., 2023; He et al., 2022), which also explains the observed positive temperature anomaly (mean: ΔT = 0.77 °C). Therefore, despite the high-pressure background, it is this extraordinarily strong localized shear and turbulent mixing, that serves as the primary mechanical driver forcing O_3 downward to the surface during WNE-type. Combined with rapid dispersion of local NO emissions under high winds that greatly mitigates nighttime titration, vigorous vertical entrainment counteracts both horizontal diffusion and titration loss of O_3, and ultimately causes a net O_3 surge.

6. In the analysis of NOI formation mechanisms, it is unreasonable to study the mechanisms of NOI occurring in different seasons together. For example, the S-type events in spring and those in autumn have vastly different precursor substances and meteorological conditions, which naturally leads to differences in the formation mechanisms of NOI.

Response 6: Thanks for reviewer's comments. The baseline meteorological conditions and chemical precursor substances (e.g., VOCs and NO_x) indeed vary profoundly across seasons. Under normal circumstances (especially regarding daytime photochemical O_3 production), analyzing different seasons together would be unreasonable.

We carefully re-evaluated our unified approach. We ultimately retained the cross-seasonal grouping based on the following specific physical and statistical considerations, which we have now better clarified in the manuscript:

(1) Isolating nocturnal physical transport from chemical production: Because our study

specifically isolates the nocturnal sudden spikes (NOI), which is a period when photochemical production ceases and rapid physical transport (e.g., downward intrusion from the residual layer) dominates the variance. We found that the overarching mechanical triggers operate somewhat independently of the seasonal chemical baselines. For instance, the mechanical shear required to break the nocturnal inversion relies on the synoptic dynamic framework. This physical mechanism remains fundamentally consistent across seasons, even though the absolute baseline O_3 concentrations and precursor emissions differ.

(2) Balancing seasonal stratification with statistical robustness: We attempted to stratify the mechanisms by season, but we encountered a practical limitation: subdividing the unified major categories into four distinct seasons severely fragmented our sample size of 171 NOI days. This fragmentation significantly weakened the statistical power of our boundary-layer anomaly tests (e.g., the ANOVA in Table S2), making it difficult to extract robust, overarching synoptic-scale signals without being overwhelmed by localized statistical noise.

(3) Empirical verification of dynamical consistency (Fig. S6): To ensure that our unified grouping did not obscure crucial seasonal differences, we conducted an additional seasonal stratification analysis specifically for the S-type (Fig. S6). The results confirmed that the underlying dynamical frameworks are functionally comparable among seasons:

Horizontal synoptic forcing: As shown in Figs. S6(a) and (b), the SLP gradient (which rigorously defines the Lamb-Jenkinson weather typing) drives a robust, seasonally consistent southerly airflow through the study region in both spring and autumn. The fundamental spatial pattern of this forcing remains unchanged.

Vertical structure of motion: Vertically, Figs. S6(c) and (d) reveal a consistent pattern of vertical motion. In both seasons, the region is dominated by prominent upward velocities.

Lines 314-320:

It should be noted that while seasonal variations significantly influence the daytime photochemical generation and absolute background concentrations of O_3, the nocturnal occurrence of NOI is predominantly driven by physical transport. As validated by the seasonal comparison (Fig. S6 and Text S3), while the absolute intensity of meteorological variables naturally fluctuates across seasons, the fundamental dynamical frameworks for a given weather type (e.g., the general orientation of horizontal pressure gradients and patterns of vertical motions) maintain functionally

comparable mechanical triggers. Therefore, rather than focusing on seasonal background variations, our study focuses on elucidating these primary, synoptically-driven local meteorological drivers that trigger NOI.

Text S3: Cross-seasonal dynamical consistency of weather types.

To demonstrate that the dynamical mechanisms driving NOI under a specific synoptic classification remain functionally consistent across different seasons, a seasonal stratification analysis was conducted for S-type (Fig. S6).

(1) Horizontal synoptic forcing: As shown in Figs. S6(a) and (b), both spring and autumn S-type are driven by a virtually identical synoptic pressure gradient: lower SLP to the west and a prominent high-pressure system to the east. This forces a robust, seasonally-consistent southerly airflow directly through the study region. The spatial pattern of forcing is fundamentally unchanged.

(2) Vertical structure of motion: Vertically, Figs. S6(c) and (d) confirm a highly consistent structure of vertical motion. In both spring and autumn, the region around Xinxiang is dominated by a prominent upward motion ($\omega < 0$).

(3) Consistency check: The only discernible difference is in the intensity. This verification definitively proves that the overarching physical triggers are functionally comparable across seasons under S-type.

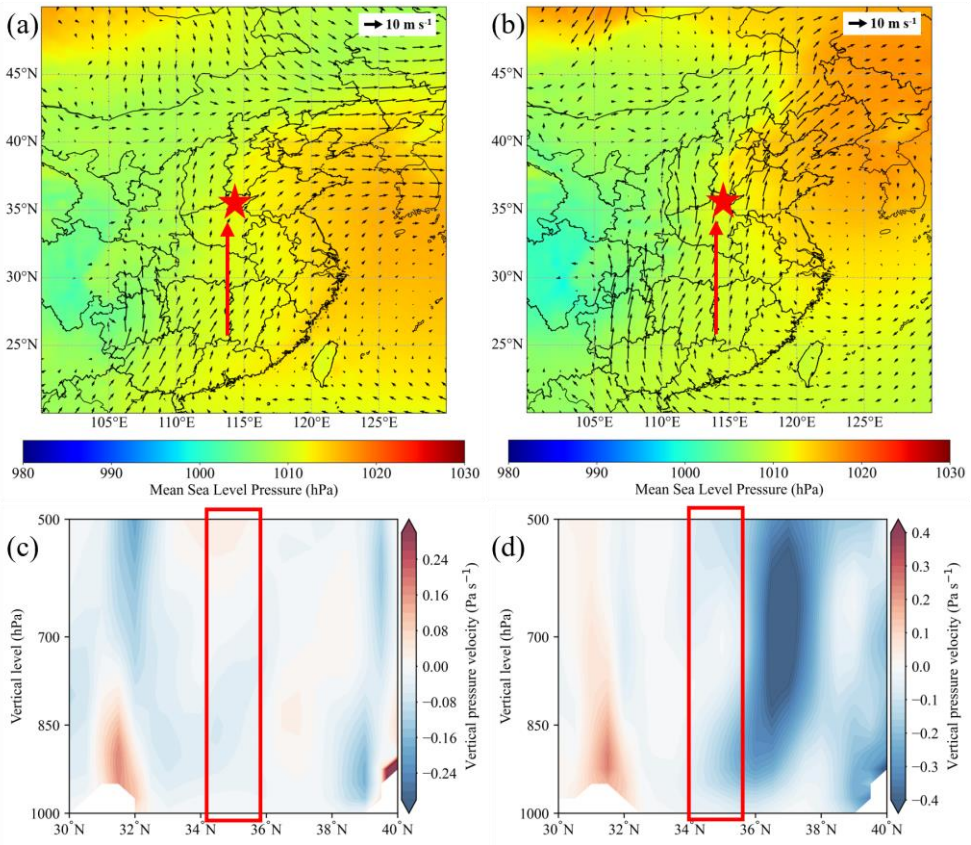

Figure S6: During spring ((a) and (c)) and autumn ((b) and (d)), spatial distribution of composite mean SLP and 850 hPa wind fields ((a) and (b)), and vertical profiles of pressure velocity ((c) and (d)) under S-type (asterisk indicates the location of Xinxiang; red rectangles indicate the region of Xinxiang). In terms of vertical pressure velocity, negative values correspond to upward motion, while positive values indicate subsidence.

Specific comments:

1. The content within the parentheses in the caption of Figure S5 is not specified.

Response 1: Thanks for reviewer's comments. The numbers in parentheses are indeed 4-digit binary codes used to indicate the occurrence status of NOI events across the four specific stations.

The four digits correspond to the occurrence of NOI in DX, XY, DY, and KF stations, respectively. A value of 1 denotes the occurrence of an NOI event at that specific station, while "0" denotes non-occurrence. For instance, (1111) indicates that the NOI event was observed simultaneously at all four stations (the cooccurrence of all four sets), whereas (1000) indicates that the event was observed only at the DX station.

We have now added this detailed explanation to the caption of Figure S5 (revised Figure 3) to

eliminate any ambiguity for the readers.

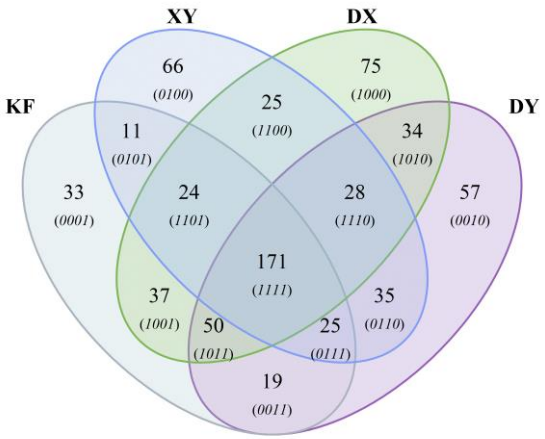

Figure 3: Overlapping occurrences of NOI days at national monitoring stations in Xinxiang, 2021-2023. The four-digit binary codes in parentheses indicate the specific occurrence status of NOI events across the four stations (in the order of DX, XY, DY, and KF). A digit of 1 represents the occurrence of the event, and 0 represents non-occurrence (e.g., (1111) denotes cooccurrence at all four stations, while (1000) denotes occurrence only at the DX station).

2. The reference to Figure 1 on line 160 does not support the explanation of the preceding sentence; please correct this. After the correction, the entire content of Section 3.1.2 is cited from the Appendix; consider incorporating some of this content from the Appendix into the main text.

Response 2: Thanks for reviewer's comments. We have revised relevant txt in manuscript.

(1) Clarification on Figure 1:

In Figure 1, the dotted line labeled "overlap" represents the "representative NOI days" (i.e., the 171 days when NOI occurred simultaneously at all four stations). As shown by this "overlap" line in Figure 1, its monthly variation trend (e.g., peaks in March and September, and dips in January and December) is consistent with the variations observed at the individual stations. We have revised the manuscript to state this connection, ensuring the text is fully supported by Figure 1.

(2) Incorporating appendix content into the main text:

Section 3.1.2 previously relied too heavily on the supplementary information. To improve the coherence and substance of the main text, we have moved the O_3 diurnal variations analysis (previously Figure S4) directly into the main text as the new Figure 2. We also moved the Venn diagram, previously Figure S5, into the main text as Figure 3.

Lines 242-244:

Furthermore, the monthly variation of these representative regional events (indicated by the "overlap" dotted line in Fig. 1) consistently matches the seasonal trends observed at individual stations (e.g., distinct peaks in March and September, and dips in January and December).

3. Lines 190–195: The authors merely state facts (e.g., Type A events occur more frequently in autumn) without linking them to the subsequent analysis of NOI mechanisms. How does this information contribute to understanding the causes of NOI?

Response 3: Thanks for reviewer's comments. Merely stating descriptive seasonal statistics of weather types without linking them to the fundamental physical mechanisms significantly weakened the narrative flow and distracted from the core focus of the paper.

Upon deep reflection on this comment, and to address reviewer's related concern regarding seasonal mechanism analysis in Comment 6, we realized that these purely descriptive seasonal breakdowns did not actively contribute to understanding the dynamic causes of NOI. As we detailed in our response to Comment 6, the overarching mechanical triggers (e.g., macroscopic wind shear and subsidence) of a given weather type remain functionally consistent across different seasons.

Therefore, to drastically improve the analytical clarity and maintain a strict focus on the physical drivers, we have completely deleted this descriptive paragraph regarding the seasonal frequencies of weather types in the revised manuscript. Instead, we have restructured the entire mechanism section to focus strictly on how the synoptic circulations govern the localized boundary-layer dynamics, eliminating the descriptive distractions. The revised Section 3.3 can be found Lines 307-367.

4. Lines 205–210 and Table S2: The analysis of meteorological conditions for each weather type here lists only averages but does not include any significance tests.

Response 4: Thanks for reviewer's comments. To address this and enhance the statistical robustness of our study, we have made the following major revisions:

(1) Removing the previous unverified averages: We have deleted the previous seasonal average analysis that lacked statistical support.

(2) Introducing rigorous ANOVA tests: We conducted a One-Way Analysis of Variance

(ANOVA) to rigorously test whether the differences in the nocturnal meteorological anomalies (T, RH, WS, PBLH and U^*) across the four weather types are statistically significant.

(3) Updating Figures and Tables: The results of the significance tests are now comprehensively visualized in the newly added Figure 6 (which displays the distributions and ANOVA results) and thoroughly detailed in the completely revised Table S2 (which now includes the statistical summary and corresponding p-values).

As shown in the updated Figure 6 and Table S2, the ANOVA tests confirm that the micro-meteorological responses to the different synoptic forcings are indeed statistically significant (typically $p < 0.01$), thereby providing a solid, quantitative foundation for our dynamical mechanism analysis in Section 3.3.

Lines 288-296:

Furthermore, to statistically confirm that these different synoptic structures translate into distinctly different local thermodynamic environments, a One-Way ANOVA was performed on the nocturnal anomalies of key meteorological variables (T, RH, WS, PBLH and U^*) across the four groups. The resulting statistical distributions and data spreads are visually compared in Fig. 6, while the precise quantitative parameters and significance test results are detailed in Table S2. To strictly isolate the meteorological perturbations driven by synoptic systems and to eliminate the influence of seasonal and interannual backgrounds, the nocturnal anomalies (Δ) for key meteorological variables were calculated as the difference between the NOI days' specific nocturnal average and the corresponding monthly nocturnal mean. The results show that the inter-group differences are highly statistically significant (all $p < 0.01$), definitively proving that our quantitative classification objectively separates fundamentally different boundary layer environments.

5. Line 220: The authors infer that the 850 hPa wind field "likely carried substantial moisture" based solely on the wind field itself. We recommend providing more direct evidence, such as calculating and presenting the 850 hPa water vapor flux and its divergence.

Response 5: Thanks for reviewer's comments. We have quantitatively calculated the 850 hPa water vapor flux and its divergence to provide direct evidence. The results are now presented in the newly added Figure S7.

As demonstrated in Figure S7, under C-type conditions, there is a prominent and intense southwesterly moisture transport belt (highlighted by the red box). Furthermore, significant moisture convergence is clearly observed along the entire path of this belt, directly encompassing the Xinxiang region (green box). This direct thermodynamic evidence robustly corroborates our previous inference, confirming that this airflow carries substantial moisture conducive to regional convection.

We have incorporated these findings into the revised manuscript to strengthen the mechanistic explanation for C-type events.

Lines 333-336:

Combined with the water vapor flux and divergence fields at 850 hPa, we find that the intense southwest warm-wet moisture transport belt under C-type is extremely prominent. Significant moisture convergence is observed along the entire path of this belt (including Xinxiang) (Fig. S7).

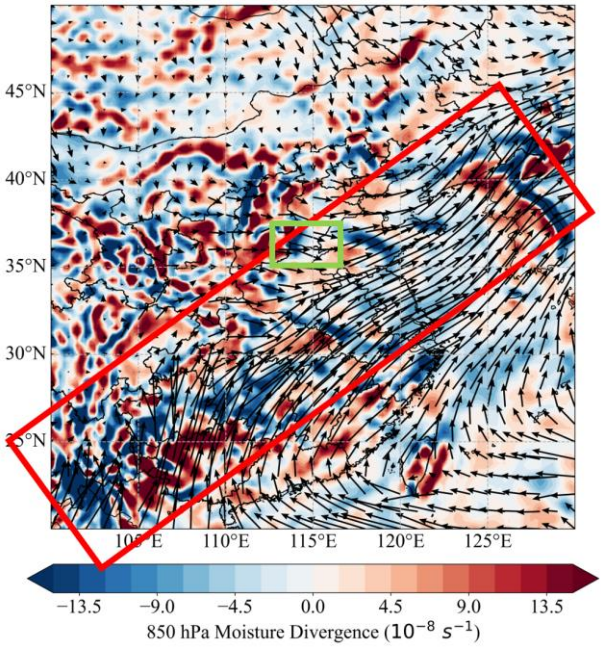

Figure S7: 850 hPa water vapor flux and divergence fields under C-type (the red box denotes the moisture transport path, corresponding to Fig. 5(b); the green box marks the Xinxiang region).